Wear 390–391 (2017) 11–22

Contents lists available at ScienceDirect

Wear

journal homepage: www.elsevier.com/locate/wear

Modeling of normal force and finishing torque considering shearing and ploughing effects in ultrasonic assisted magnetic abrasive finishing process with sintered magnetic abrasive powder

Vipin C. Shukla[a], Pulak M. Pandey[a,*], Uday S. Dixit[b], Anish Roy[c], Vadim Silberschmidt[c]

[a] Department of Mechanical Engineering, IIT Delhi, India
[b] Department of Mechanical Engineering, IIT Guwahati, India
[c] Wolfson School of Mechanical and Manufacturing Engineering, Loughborough University, UK

ARTICLE INFO

Keywords:
UAMAF
Shearing
Ploughing
Force
Torque
Wear

ABSTRACT

Ultrasonic assisted magnetic abrasive finishing process (UAMAF) is a precision manufacturing process that results nano-scale level finish in a part. Normal force on a particle helps indenting the particle in the work surface whereas horizontal force provides finishing torque that in-turn helps the particle to perform micro-machining. Better understanding of the effect of these forces on material removal and wear pattern of the work-piece necessitates mathematical modeling of normal force and finishing torque and subsequently its validation with experimental results. In the present study, single particle interaction concept is considered to develop a model which is subsequently applied for all active particles of magnetic abrasive powder (MAP). Separation point theory is applied to consider the effect of ploughing below a critical depth and shearing above that depth. Normal components of shearing and ploughing forces are considered for calculating normal force and horizontal components of shearing and ploughing forces are taken to calculate finishing torque. Johnson-Cook model is applied to calculate shearing strength of the work material during UAMAF. The impact of ultrasonic vibrations is considered while calculating strain rate. Images are taken with the help of scanned electron microscope and atomic force microscope to study the material removal and wear mechanism during UAMAF process. Predicted values of force and torque model are validated with the experimental values.

1. Introduction

Latest trends in manufacturing sector have opened new research avenues for extensive applications of advanced engineering materials, high quality geometrically complex parts and requirement of nano level finishing. Application of materials with superior properties and desire of high quality dimensional complex parts have necessitated industries to move from micro to nano level research. Use of rigid tools in traditional machining processes may cause micro-cracks or any other defects in the part due to the substantial normal force generated during machining process. Due to the rigidity of tool, finishing of intricate geometrical parts is also challenging. Challenges to finish advanced materials under gentle force conditions and intricate geometrical parts are overcome to a great extent by using non-traditional machining processes. Many magnetic field assisted non-traditional techniques have shown encouraging results in achieving better surface finish and defect-free parts as the forces and torque required in these techniques are controllable within a desirable range by using an external magnetic field [1,2]. Ultrasonic assisted magnetic abrasive finishing (UAMAF) is one of the magnetic field assisted non-traditional techniques where surface finish is achieved by a flexible magnetic abrasive brush (FMAB) developed by ferromagnetic iron and non-ferromagnetic abrasive particles (called magnetic abrasive powder or MAP) in presence of magnetic field and ultrasonic vibrations [3,4].

Significance of various forces acting on the work-piece and their effect in case of traditional machining processes have been studied widely by carrying out experimental investigations and modeling the material removal, wear behaviour, forces etc. based on shearing effect. UAMAF or magnetic abrasive finishing (MAF) process is a relatively recent advancement among non-traditional finishing techniques which requires a thorough mathematical model for the prediction of forces/torque and its effect on material removal/wear. Jayaswal et al. [1] carried out theoretical investigations into MAF process by developing a finite element model and evaluated magnetic forces. It was concluded in this study that the process removed material from the work surface due to indentation and rotation of MAP in circular tracks. Singh et al.

* Corresponding author.
E-mail address: pmpandey@mech.iitd.ac.in (P.M. Pandey).

http://dx.doi.org/10.1016/j.wear.2017.06.017
Received 14 February 2017; Received in revised form 24 June 2017; Accepted 25 June 2017
Available online 27 June 2017

Nomenclature

A / B / C / m / $\ddot{n}$	constants in Johnson-Cook model
A_L	cross-sectional area of different length of equivalent magnetic circuit
A_{poles}	cross-sectional area of all electromagnet poles
A_s	area sheared by single bulge
A_Z	cross-sectional area of FMAB
B_z	magnetic flux density in working gap
d	distance between particles on adjacent tracks
d_{SiC}	diameter of SiC particles
F	magnetomotive force
F_y	total normal force
f	Frequency of ultrasonic vibrations
$\dot{f}_y$	normal force on a single SiC particle
f_y	normal force on a single bulge
$\dot{f}_{sx}$	shearing force in horizontal direction on single SiC particle
f_{sx}	shearing force in horizontal direction on single bulge
$\dot{f}_{px}$	ploughing force in horizontal direction on single SiC particle
f_{px}	ploughing force in horizontal direction on single bulge
F_{py}	total ploughing force in vertical direction
f_{py}	ploughing force in vertical direction on single bulge
H	Brinell hardness number for work-piece
I	current in electromagnet
n	number of circular tracks under electromagnet
n_b	number of bulges (in a single SiC particle) indented in the workpiece
n_l / n_w	number of active SiC particles along the length / width of pole
N	number of turns in coil
N_b	total number of abrasive bulges (for all active particles) indented in the workpiece
N_{Fe} / N_{SiC}	number of iron / SiC particles in bottom most layer of FMAB
P	polishing pressure
r_{Fe} /r_{SiC} / r_b	radius of iron particle / SiC particle / bulge
r_n	radial distance of SiC particle in first circular track from centre of electromagnet
R_A /R_c / R_G / R_W	reluctance of circuit against return flux flow in air / core / working gap / work-piece
t	total depth of cut due to indentation
t_s	depth of cut due to shearing effect
t_p	depth of cut due to ploughing effect
T / T_m / T_r	working temperature / melting temperature / room temperature
V_i	volume fraction of iron particles in sintered MAP
T_f	total finishing torque
T_g	finishing torque due to single SiC particle
T_{on} / T_{off}	Ultrasonic on / off time
V	Total cutting velocity of a single active particle
v_c / v_u	velocity due to rotation of electromagnet / ultrasonic vibrations
w	width of the indentation
W	total weight of MAP
z	working gap
α	rake angle
α_{cr}	critical rake angle
β	friction angle
ϵ	equivalent plastic strain
$\dot{\epsilon}$	equivalent plastic strain rate
λ	Wavelength of ultrasonic vibrations
μ_p	friction coefficient in ploughing zone
μ_0	permeability of vacuum
μ_r	relative permeability of a medium
τ_s	shear strength of work-piece
φ	total flux flow in circuit
$\varnothing$	shear angle

[5] analysed wear behaviour, material removal mechanism and normal force involved during the ball end magnetorheological finishing process by developing mathematical model and performing experiments. Mulik et al. [6] measured the force responsible for indention and the torque responsible for cutting the peaks of work surface during UAMAF process to understand the effect of various process parameters and also developed a mathematical model based on shearing effect for comparing it with the results of experiments. Kala et al. [7] performed experimental study on the finishing forces on paramagnetic work-piece in double disk MAF process. All these researchers [1,5–7] considered shearing effect while developing the theoretical models and did not take ploughing phenomenon into consideration.

Park et al. [8,9] carried out force modeling of micro-grinding process considering both cutting and ploughing phenomena based on single grit interaction analysis to estimate the material deformation and micro-grinding forces. Micro-cutting and ploughing force components in cutting and thrust directions were worked out mathematically for computing total thrust and cutting forces. Ploughing effect was compared with micro-cutting effect in both thrust and cutting directions. The analytical model was validated with experimental investigations also. Sin et al. [10] carried out experimental and theoretical work to study abrasive wear mechanism and the grit size effect including the effect of ploughing. It was found that the theoretical wear coefficient was more than the experimental wear coefficient and bluntness of the abrasive particles affected wear and friction mechanism. Son et al. [11] carried out theoretical and experimental investigations in micro-cutting and studied relationship between friction and minimum cutting thickness. During machining operation of work-piece with blunt tools, Basuray et al. [12] studied the shifting of phase from ploughing to cutting and determined a value for neutral point angle in relation to the critical depth of cut. Popov et al. [13] compared different methods for determining ploughing force in orthogonal cutting process. Waldorf et al. [14] made analytical comparison between two basic ploughing models, one based on assumption of presence of a separation point on the rounded cutting edge and other on a stable build-up adhered to the edge. Force components in the cutting (horizontal) and thrust (vertical) directions due to shear and plough phenomenon were calculated by developing theoretical models and theoretical predictions of ploughing components were compared. Germain et al. [15] reviewed work performed in the area of force modeling in metal cutting processes including ploughing effect. This review was carried out on different approaches based on empirical, mechanistic and analytical models. Snahungshu et al. [16] modeled the force for composite materials undergoing machining operation and studied the impact of particle size on the forces. Different cutting mechanics like shearing, ploughing and particle fracture were considered. Resultant cutting force and thrust force were proposed by summing up respective components of shear, plough and particle fracture forces while developing the force model. The analytical model was subsequently compared with experimental results. Singh et al. [17] developed theoretical models for estimating specific grinding energy considering chip formation energy, rubbing and ploughing energy.

Above literature review reveals that researchers [1,5–7] carried out theoretical and mathematical studies of MAF/UAMAF process considering shear but not plough effect. These researchers used mechanically mixed powder for their experimental work. Researchers [8–17] studied traditional machining processes considering both the shear and plough phenomena. In nutshell, it is concluded that MAF/UAMAF

process requires an extensive theoretical study and development of a mathematical model considering both shearing and ploughing effects together to understand the micro-cutting mechanism and wear pattern. In the present work, theoretical model of Fe-SiC abrasive particles arrangement for sintered MAP was proposed to calculate possible active number of particles involved in the finishing action. Based on this, a mathematical model of normal force and finishing torque was developed. Effect of ploughing phenomenon on these force and torque was also studied. Normal force was induced due to the magnetic field and hence total flux generated by continuous direct current was estimated. Further, experiments were performed to validate the mathematical models and to understand the contribution of wear mechanism on the surface finish.

2. Experimental set-up

A complete set-up was developed to fix the work-piece (work material SS304) on a CNC milling machine with a provision to hold ultrasonic horn for transmitting horizontal vibrations to the work-piece. An electromagnet fixed in the spindle of the milling machine was coupled with a direct current power supply. The measurement of desired force and torque for UAMAF process was done by mounting the work-piece holder setup on a dynamometer (Schunk Delta SI330-30) as shown in the Fig. 1. A set of power source, piezoelectric transducer with a horn constituted a complete unit of an ultrasonic vibration generator setup which produced electrical signals. These signals were then transmitted to the piezoelectric crystals inside the transducer. This transducer changed the electrical signals of 20 kHz into the mechanical vibrations, which were subsequently transmitted to the work-piece when the work-piece maintained a contact with the horn.

3. Mathematical modeling of normal force and finishing torque

Iron particles and abrasive particles (SiC) are sintered in a high temperature tube furnace to produce bonded MAP where a number of smaller sized SiC particles are diffused on the bigger sized iron particles. It is assumed that all iron particles are identical and the same holds good for SiC particles also. The shapes of both iron and SiC particles are considered to be spherical, however the SiC spherical particle is assumed to be made of a number of small bulges spread all over the surface as depicted in Fig. 2(a) [18]. These bulges in the SiC particle are effective in cutting and finishing actions. All abrasive particles do not take part in cutting/finishing action. In this work, it has been assumed that whole amount of MAP is kept in between magnetic poles and work-piece surface only and effective cross-sectional area of FMAB formed is equal to the cross-sectional area of pole as displayed in Fig. 2(b). Flux leakage and copper losses during finishing are not considered. The magnetic field intensity in the working zone does not vary with time and is uniform in the machining or finishing gap.

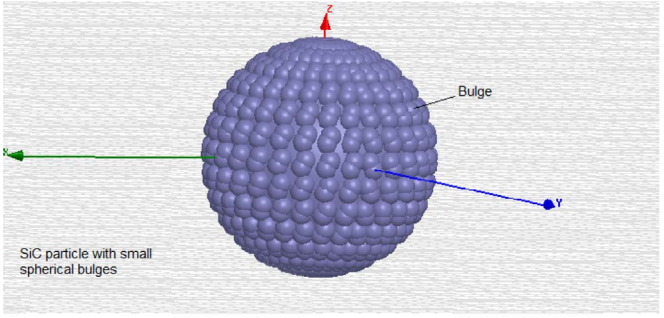

(a)

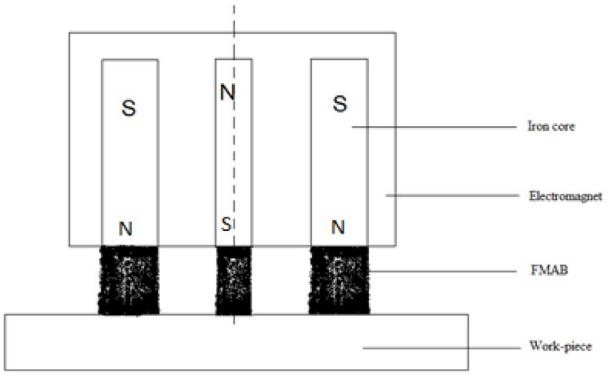

(b)

Fig. 2. (a) Single SiC particle with bulges, (b) Schematic diagram of FMAB between poles and work-piece.

3.1. Estimation of active abrasive particles in MAP

It is assumed that the bottom-most layer of MAP is involved in finishing process, which is considered as a layer of active particles. A number of bulges on SiC particles of this layer are indented in the work-piece under the action of normal force. The indentation of a bulge of a single active SiC abrasive particle is depicted in Fig. 3(a). Further it is assumed that a bulge is hemispherical in shape and this hemispherical bulge is involved in indentation process. A single particle of SiC has radius r_{SiC} and bulge has radius r_b as shown in Fig. 3(a). These small bulges play a key role in micro-finishing and radius r_b is assumed as cutting edge radius. Most of the ceramics including SiC are polycrystalline materials consisting of many crystallites that are randomly oriented with respect to each other. Crystallites, made of many number of crystals, are also referred to grains and grain boundaries are the interfaces where crystals of different orientations meet. It is assumed that a bulge on any SiC grit is equivalent to a crystallite. For calculating the crystallite size of SiC particle, XRD analysis of the sintered MAP is carried out and peak broadening effect due to crystallize size and strain

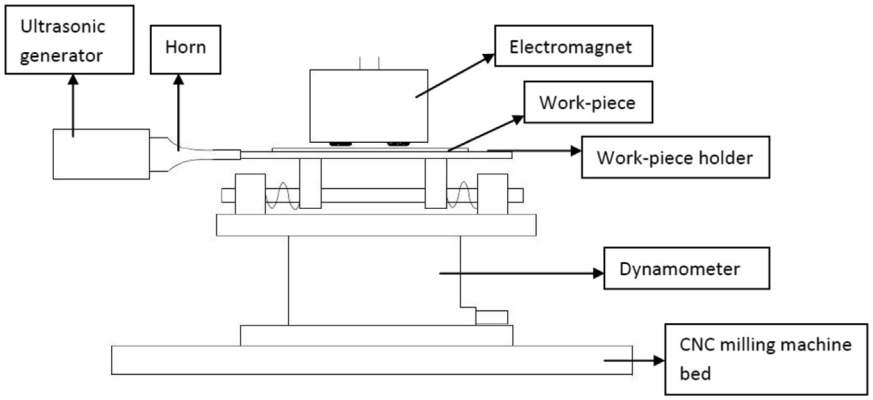

Fig. 1. Schematic diagram for complete arrangement.

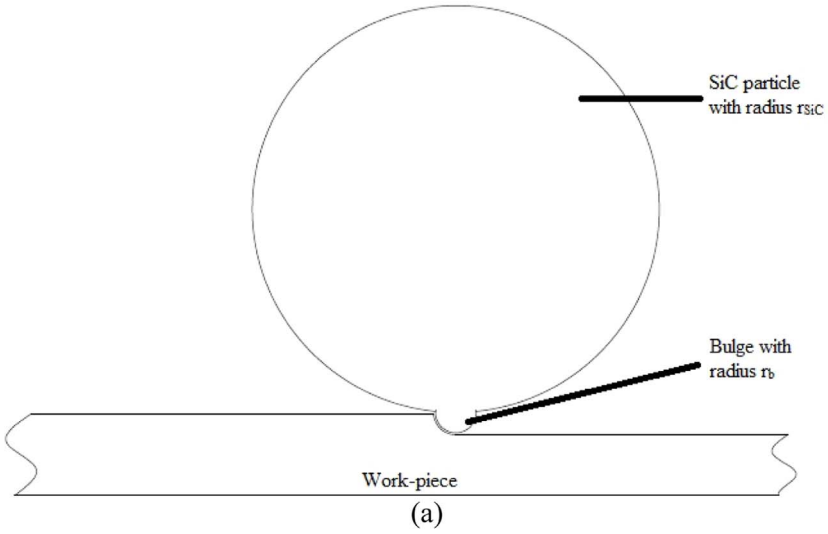

(a)

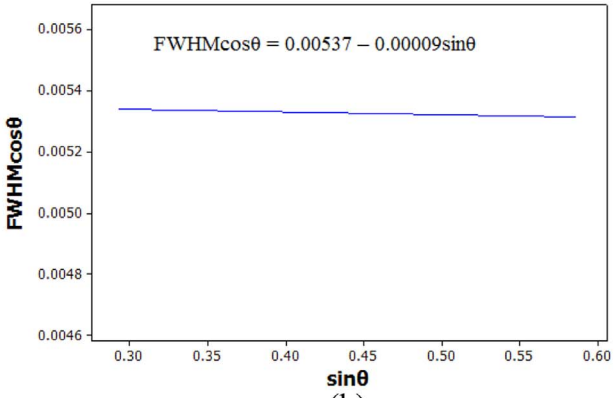

(b)

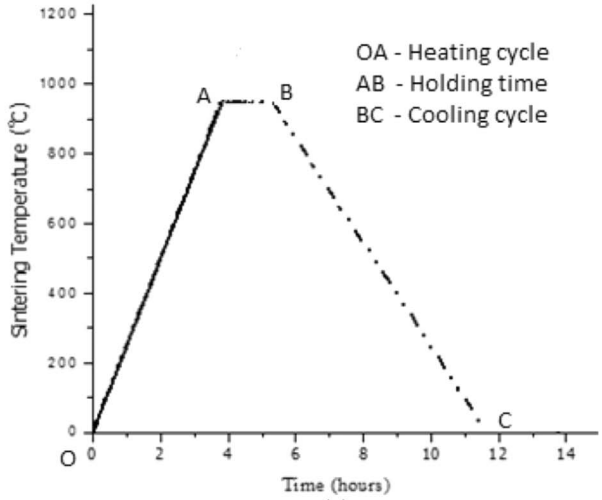

(c)

Fig. 3. (a) Single SiC particle with a bulge indenting in the work piece, (b) Williamson-Hall plot for SiC [19]. (c) Complete sintering cycle for preparation of MAP.

Table 1
Details of constituents of MAP.

Material	Weight (gm)	Density (gm/cm^3)	Volume (cm^3)	Mesh size (μm)
Fe	0.75 W	7.8	0.75 W/7.8	49
SiC	0.25 W	3.21	0.25 W/3.21	22

factors are studied as per the following equation:

$$FWHM\ \cos\theta = (k\lambda/L) + 4\epsilon sin\theta \quad (1)$$

where $FWHM$ is the full width at half maximum, k the Scherrer's constant (=1), λ the wavelength of Cu-K_α radiation (=1.54056 Å), L the crystallite size in Å, θ the diffraction angle and ϵ denotes strain in the material. Williamson-Hall plot for SiC particles is drawn in Fig. 3(b) to calculate the crystallite size. It is calculated from the plot that average crystallite size of SiC particles is 30 nm which is taken as the

Table 2
Material properties and machining conditions.

Work-piece material	SS304
Dimension of workpiece sample	100 × 100 × 2 (mm)
Hardness of the work-piece (*BHN*)	431
Radius of magnet	40 mm
Radius of iron particle	24.5 μm
Radius of SiC particle	11 μm
Diameter of bulge	30 nm
Relative permeability of electromagnet core material	5000
Relative permeability of SS304 work material	1
Permeability of vacuum	$4\pi\times10^{-7}$ H/m
Number of turns in coil	480
Area of poles	600 mm^2
Frequency of ultrasonic horn	20000 Hz
Amplitude of ultrasonic vibration	20 μm

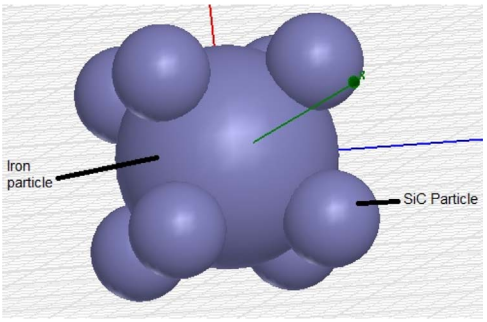

Fig. 4. Single sintered magnetic abrasive particle.

diameter of a bulge.

To understand the effect of various process parameters on magnetization of sintered MAP, a parametric study was carried out by designing the experiments. The optimum values of sintering temperature, holding time, percentage of iron particles and percentage of SiC particles that achieved maximum magnetization of sintered MAP were taken in the present study [3]. Based on the optimized values, sintered MAP containing 75% Fe and 25% SiC by weight was taken in the present study. Total weight of MAP is considered as W for calculation purpose. Sintering temperature and holding time for the sintering of iron and SiC particles were taken as 950 °C and 1.5 h, respectively. Fig. 3(c) depicts the complete sintering cycle which also reflects heating, holding and cooling time. Table 1 summarizes details about volume of iron and abrasive particles in MAP and Table 2 provides details regarding the properties of work-piece material, abrasive material and the machining conditions.

$$\text{Volume of single i ron particle } V_{Fe} = 4\pi r_{Fe}^3/3 \tag{2}$$

$$\text{Volume of single abrasive particle } V_{SiC} = 4\pi r_{SiC}^3/3 \tag{3}$$

Ratio between number of SiC and iron particles can be calculated as

$$N_{SiC}/N_{Fe} = 0.8(r_{Fe}/r_{SiC})^3 \tag{4}$$

From Eq. (4), the ratio between number of SiC and iron particles is obtained as 8.9 and therefore it is assumed that an iron particle is surrounded by 8–9 SiC particles uniformly on its spherical surface after sintering. Based on this, it is assumed in this study that each iron particle of sintered MAP is surrounded by eight SiC particles uniformly and rested on four smaller SiC particles as shown in the Fig. 4.

Effective diameter of single sintered MAP:

$$d_{eff} = (d_{Fe}+2d_{SiC})\cos 45° \tag{5}$$

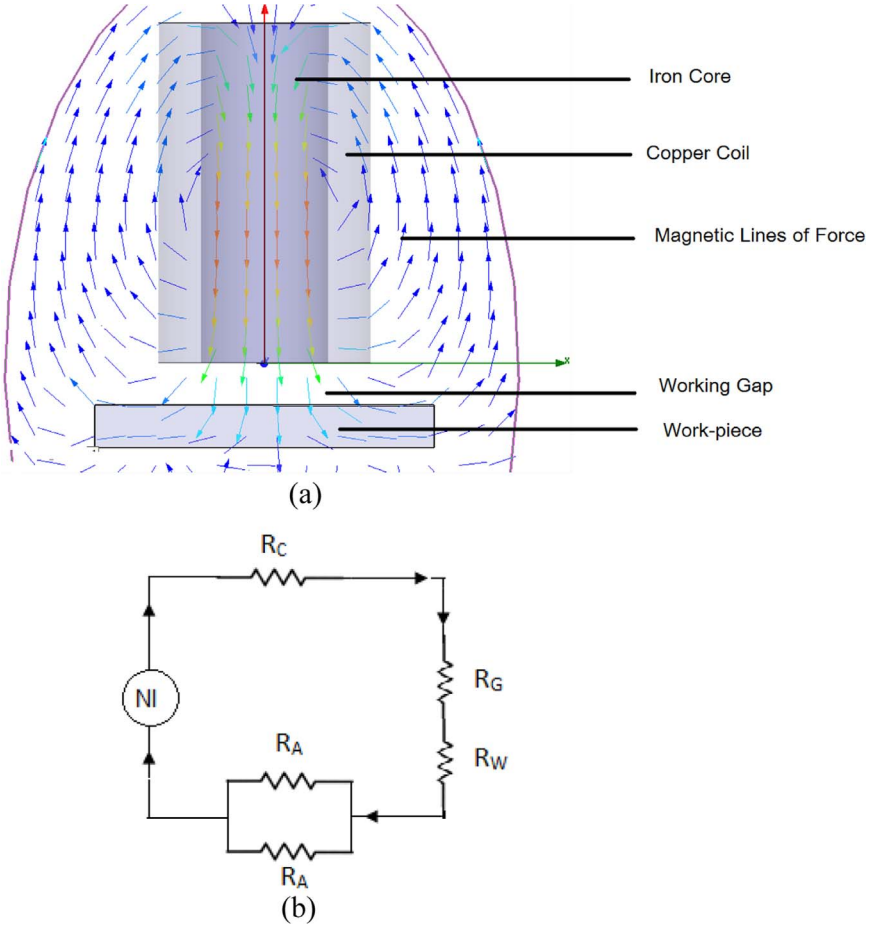

Fig. 5. (a) Schematic diagram of flux flow, (b) Equivalent magnetic circuit.

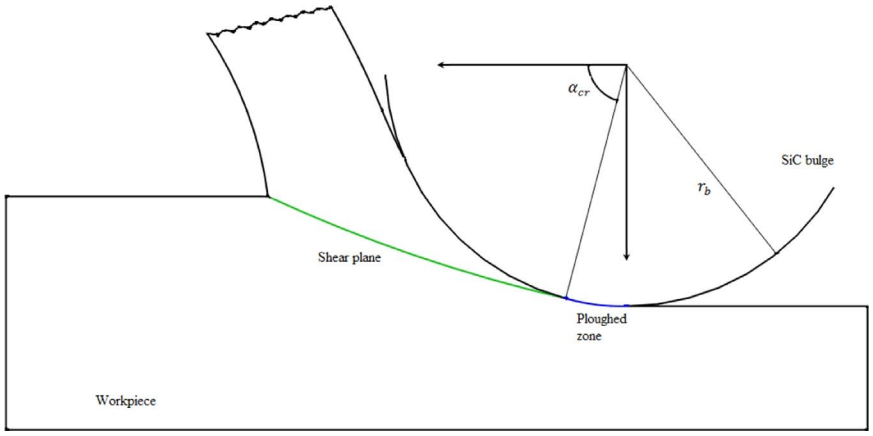

Fig. 6. Schematic diagram of effect of shear and plough phenomenon on a single bulge of SiC.

Number of iron particles in the layer just above to the work piece can be calculated as

$$N_{Fe} = A_{Poles}/S \tag{6}$$

where S is the projected area of single MAP ($= \pi d_{eff}^2/4$) and A_{Poles} is total area under all the poles. From Fig. 4, it is seen that each iron particle in a plane rests on four SiC particles, hence total number of SiC particles in the bottom-most layer is given by

$$N_{SiC} = 4N_{Fe} \tag{7}$$

If the normal force on single SiC particle ($\dot{f}_y$) produces an indentation depth of t, the normal force on single SiC particle and the hardness of the work-piece material can be expressed as [1]:

$$H = \dot{f}_y/\pi d_{SiC}\, t \tag{8}$$

Since total normal force is F_y, depth of indentation t can be calculated by

$$t = F_y/H\pi d_{SiC}\, N_{SiC} \tag{9}$$

$$\text{Surface area of SiC particle indented into workpiece} = 2\pi r_{SiC}\, t \tag{10}$$

$$\text{Projected area of single bulge on the surface of SiC} = \pi r_b^2 \tag{11}$$

Hence number of bulges of single SiC particle indented in the work-piece

$$n_b = 2\pi r_{SiC}\, t/\pi r_b^2 \tag{12}$$

Total number of bulges for all SiC active particles

$$N_b = n_b N_{SiC} \tag{13}$$

As total normal force is uniformly shared by each bulge, the normal force on a single bulge

$$f_y = F_y/N_b \tag{14}$$

3.2. Calculation of magnetic flux and polishing pressure

For calculating magnetic flux and polishing pressure, the assumptions mentioned earlier are considered. As shown in Fig. 2(b) when the magnetic field is established, MAP is densely filled in between the electromagnet and work sample for forming FMAB. The effective part of FMAB involved in finishing process is below the magnetic pole with cross-sectional area A_z. Cross-sectional area of mean length of the flux path in the work-piece is also considered equal to A_z. When the electromagnet is energised, the flux generated starts moving inside the iron core. This flux flow then passes through the FMAB which is formed in the working gap. It is assumed that flux emanating from FMAB enters the work-piece and subsequently comes out from work-piece to air and strongest magnetic lines of return flux are emanating from side and top surfaces of the work-piece. A schematic diagram of complete magnetic flux flow is drawn in Fig. 5(a) and an equivalent magnetic circuit based on this flux flow cycle is shown in Fig. 5(b).

Total flux can be calculated as per the Hopkinson's law, also known as the magnetic analogy to the Ohm's law. Magnetomotive force F is the cause of magnetic flux in the equivalent circuit and expressed as

$$F = \varphi R \tag{15}$$

where φ is the magnetic flux and R represents the magnetic reluctance which is like the resistance in an electrical circuit and can be calculated as

$$R = L/\mu_0\mu_r A_L \tag{16}$$

It is also known that value of F depends on the number of coil-turns (N) and current (I), which can again be expressed as

$$F = NI \tag{17}$$

From Eqs. (15) and (17), total flux generated can be calculated as

$$\varphi = NI/R \tag{18}$$

From the circuit given in Fig. 5(b), resultant reluctance R can be given as

$$R = R_C + R_G + R_W + 0.5R_A \tag{19}$$

Therefore,

$$\varphi = NI/(R_C + R_G + R_W + 0.5R_A) \tag{20}$$

Hence,

$$B_z = \varphi/A_Z \tag{21}$$

$$B_z = I/(2.85 + 361.91z) \tag{22}$$

B_z expressed in Eq. (22) is the magnetic flux density produced in the gap z wherein MAP is filled and it decreases with an increase in the value of z. The polishing pressure P on the work surface can be expressed by [20]

$$P = (B_z^2/2\mu_0)[1-(1/\mu_{rz})] \tag{23}$$

where μ_{rz} is the relative permeability of FMAB given by

$$\mu_{rz} = [2+\mu_{rFe}-2(1-\mu_{rFe})V_{Fe}]/[2+\mu_{rFe} + (1-\mu_{rFe})V_{Fe}] \tag{24}$$

3.3. Modeling of normal force

Polishing pressure on the work-piece surface under FMAB applies normal force which can be calculated as

$$F_y = PA_{Poles} \tag{25}$$

This normal force is assumed to be distributed uniformly among all effective bulges involved in finishing process. Single bulge under normal force is indented into the work surface creating a total depth of

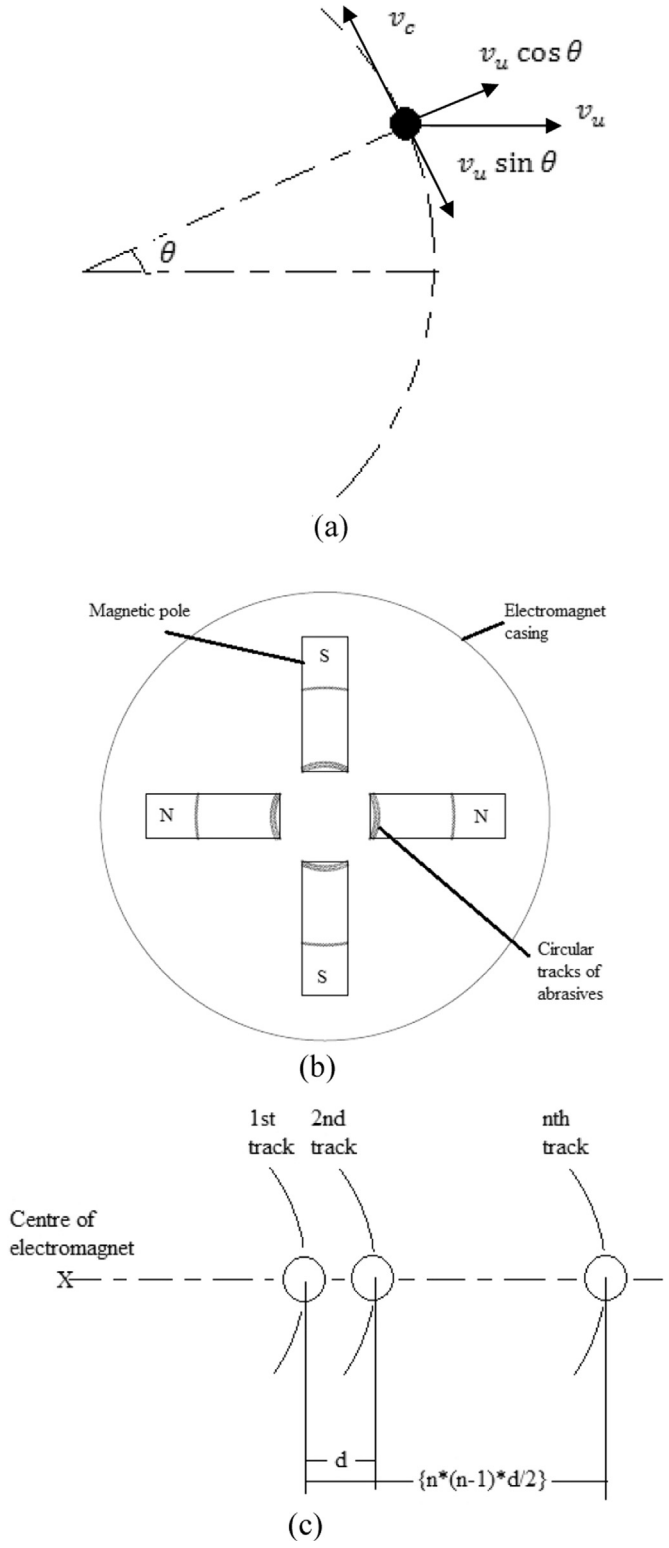

Fig. 7. (a) Schematic diagram for calculating total cutting velocity, (b) Schematic diagram of electromagnet with circular tracks, (c) Active SiC particles on circular tracks.

Table 3
Values of constants for Johnson-Cook model (Work material SS304) [26].

A	*B*	*ï*	*C*	*m*
209.696	1383.2	0.9151	−0.0095	0.5147

Table 4
Values of various temperatures.

Material temperature (°C)	Room temperature (°C)	Melting temperature (°C)
46	25	1425

cut t. In this nano-level finishing process with spherical bulges, it is assumed that ploughing effect is also present considerably in addition to the prominent shearing effect as spherical (rounded) shape provides negative rake angle which is main cause of ploughing effect [12,16,21]. Rake angle varies as per the depth of cut and a critical rake angle α_{cr} signifies a transition point from shearing to ploughing. In other words, α_{cr} is assumed as the rake angle below that the work-piece material undergoes the ploughing effect [8,9]. In this situation, the work material is compressed plastically without chip formation underneath the minimum undeformed depth of cut. It is assumed here that each particle undergoes both shearing and ploughing phenomenon. A schematic diagram of the workpiece under shearing and ploughing effects during UAMAF has been depicted in Fig. 6. The zones under shearing and ploughing effects are shown in green and blue colours respectively in Fig. 6.

Total depth of cut t due to normal force is the sum of depth of cut due to shearing t_s and ploughing t_p (for the condition $t<r_b$). In case of $t\geq r_b$, it will be assumed that single bulge will indent fully i.e., upto r_b depth in the work-piece. While proposing mathematical models, researchers [8,9,14,16] have computed total vertical (thrust) and horizontal (cutting) forces by considering respective components of shearing and ploughing forces. In ploughing region, friction due to relative movement between bulge and work piece is also taken into consideration in addition to ploughing force. The ploughing force along the direction of critical rake angle on a single bulge is f_p with f_{px} and f_{py} as horizontal and normal components. Ploughing force can be estimated as per the equation given below [8]:

$$f_p = H\pi d_b t_p \tag{26}$$

Ikawa et al. [22] performed experiments as well as computer simulations to study the relation pattern between the cutting edge and the minimum depth of cut. It was found that no stable chip formation was possible below a critical minimum depth of cut that was in the range of one tenth of the cutting edge radius. Through their theoretical model, Basuray et al. [12] predicted that a stagnation point (neutral point) to be 37.6°, which gave value of critical rake angle equal to 53.4°. This concluded that the value of minimum depth of cut was two tenth of the cutting edge radius.

Minimum depth of cut is taken as one tenth value of the cutting edge corresponding to α_{cr} for ploughing effect [8,22] in this study. Critical rake angle α_{cr} is given as:

$$\alpha_{cr} = \sin^{-1}[(r_b - t_p)/r_b] \tag{27}$$

The normal and horizontal components of ploughing force are resolved as [9]

$$f_{py} = f_p \sin\alpha_{cr} + \mu_p f_p \cos\alpha_{cr} \tag{28}$$

$$f_{px} = f_p \cos\alpha_{cr} - \mu_p f_p \sin\alpha_{cr} \tag{29}$$

where coefficient of friction for ploughing region can be taken as [10]

$$\mu_p = (2/\pi)[(w/r_b)^{-2}\sin^{-1}(w/r_b) - \sqrt{(w/r_b)^{-2}-1}\,] \tag{30}$$

3.4. Modeling of finishing torque

Component of shearing force in horizontal direction is estimated by Eq. (42) where the shear strength of the work-piece is calculated with the help of Johnson-Cook model considering various effects like strain hardening, strain rate and temperature [23]. Eq. (37) represents the

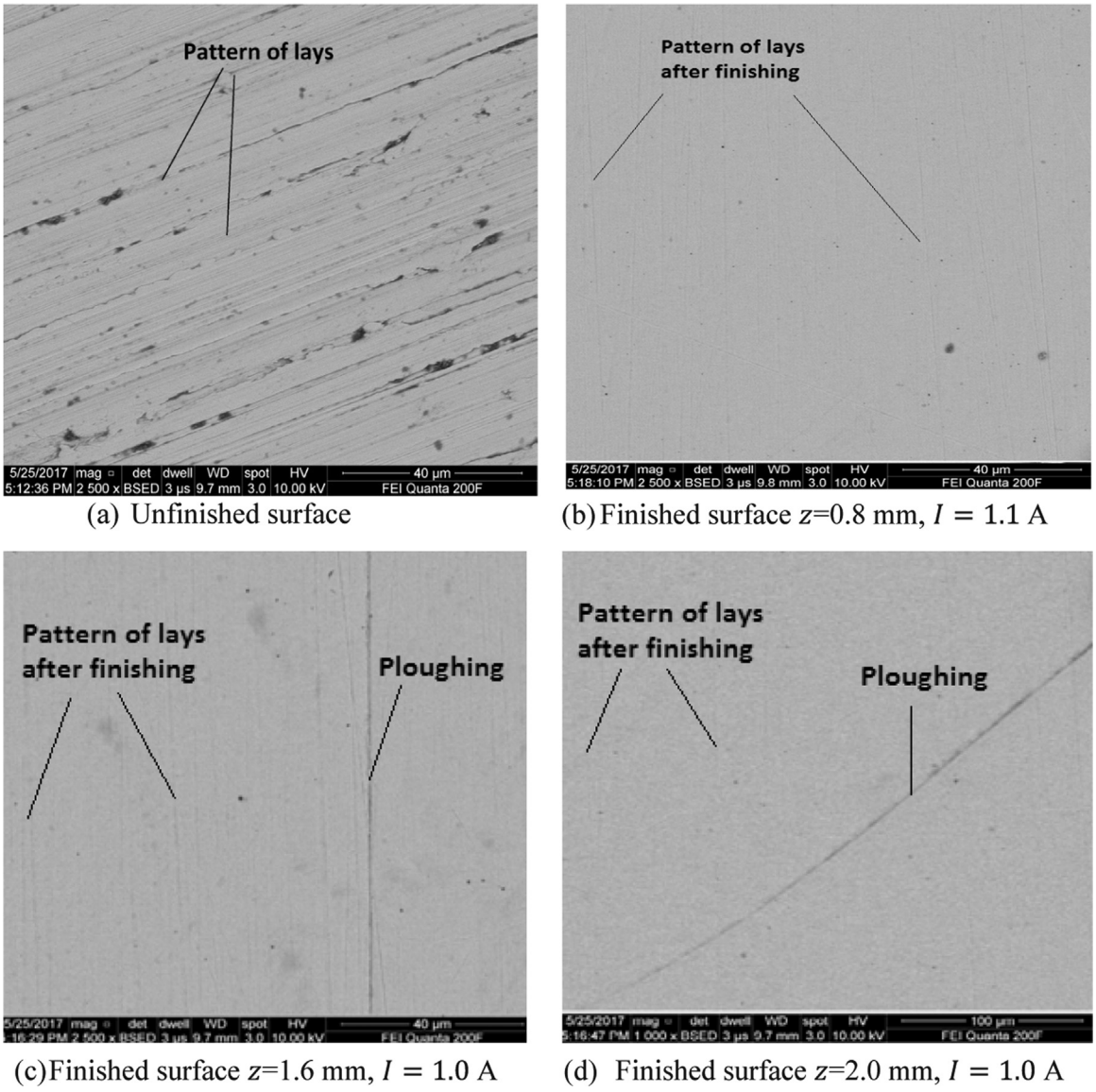

Fig. 8. SEM images for (a) unfinished; (b), (c) and (d) for finished work surfaces.

relation in this model. The effect of ultrasonic vibrations in horizontal direction is incorporated while calculating strain rate as given in Eq. (38). Strain and strain rate are calculated as per the Eqs. (38) and (39) [16]. Total cutting velocity V which is considered as cumulative effect (vector sum) of cutting velocity due to the rpm of the electromagnet and the velocity due to the ultrasonic vibrations are estimated by the researchers [5,24,25]. During UAMAF process, a single particle has two motions, one due to the rotation of electromagnet and other due to ultrasonic motion of work-piece as shown in Fig. 7(a). Total cutting velocity V can be expressed in terms of v_c and v_u as

$$\overrightarrow{V} = \overrightarrow{v_c} + \overrightarrow{v_u} \tag{31}$$

Two components of v_u are resolved, one along the direction of v_c and other perpendicular to it as shown in Fig. 7(a). These two velocities v_c and v_u can be expressed as

$$v_{c\,=}\, \pi d N_p/60000 \tag{32}$$

$$v_u = \lambda f \tag{33}$$

where d, N_p, λ and f represent diameter of the circular track wherein the particle is placed, rotation per minute of the electromagnet, wavelength of ultrasonic waves and frequency of waves respectively. From Fig. 7(a), total cutting velocity V is expressed as

$$V = \sqrt{(\overrightarrow{v_c} + \overrightarrow{v_u}\sin\theta)^2 + (\overrightarrow{v_u}\cos\theta)^2} \tag{34}$$

Considering average value of $\sin\theta$ as zero in a complete cycle of ultrasonic wave:

$$V \sim \sqrt{v_c^2 + v_u^2} \tag{35}$$

In case no ultrasonic vibrations are applied, V is due to the rotation of electromagnet only. As the ultrasonic pulse on and off time are equal, i.e., 2 s in the present study, the average value of V is given by

$$V = (1/2)(\sqrt{v_c^2 + v_u^2} + v_c) \tag{36}$$

Johnson-Cook model is given by

$$\tau_s = (1/\sqrt{3})\left(A + B\epsilon^{\bar{n}}\right)(1+C\ln\dot{\epsilon})\{1-[(T - T_r)/(T_m - T_r)]^m\} \tag{37}$$

where

$$\dot{\epsilon} = 2.59 V \epsilon \sin\varnothing/t \tag{38}$$

and

$$\epsilon = (1/2\sqrt{3})[\cos\gamma/\sin\varnothing\cos(\varnothing-\gamma)] \tag{39}$$

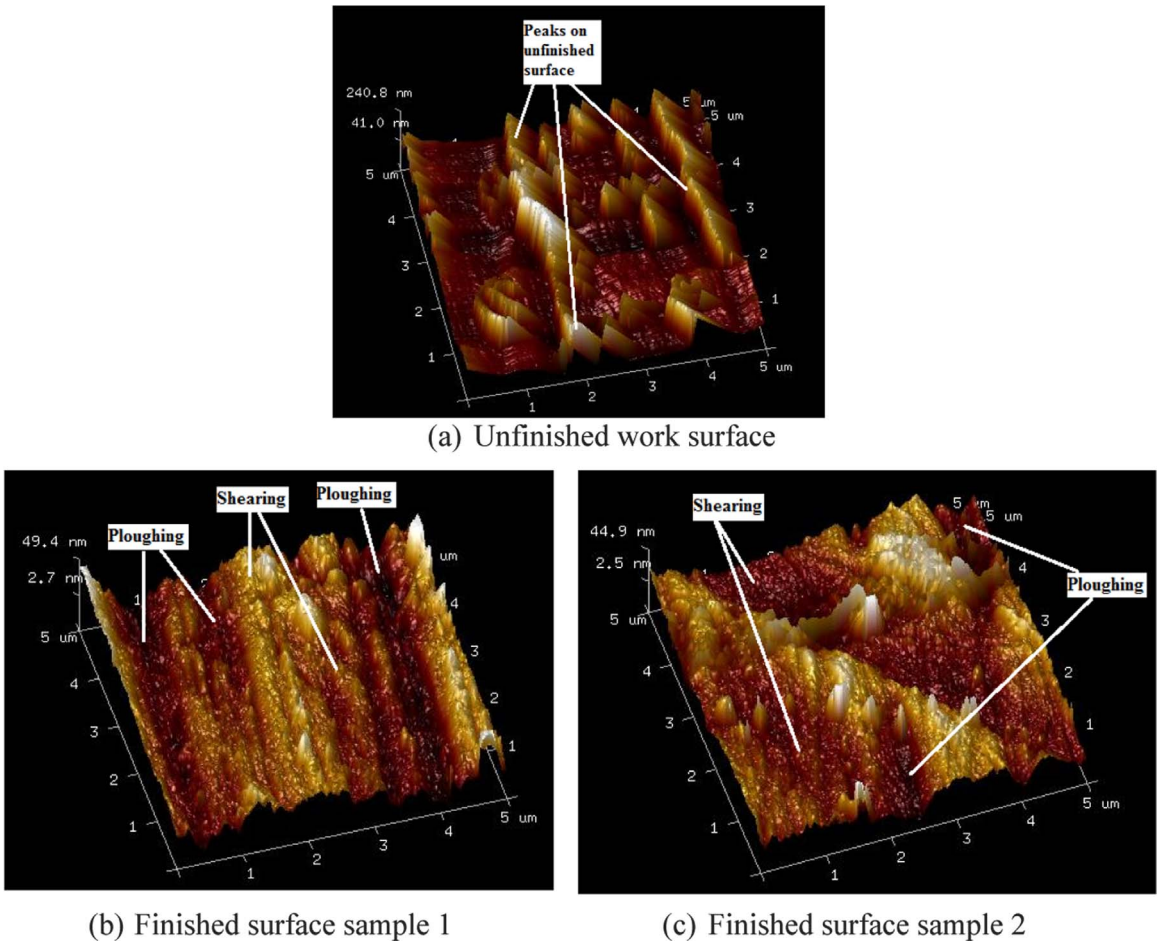

(a) Unfinished work surface

(b) Finished surface sample 1

(c) Finished surface sample 2

Fig. 9. AFM images showing shearing and ploughing effects on different samples.

Various constants in Eq. (37) of Johnson-Cook model for work material SS304 are considered with the values given in Table 3 [26]. The level of temperature at the work-brush interface is an important factor as it may affect the process mechanism and surface integrity. Mishra et al. [27] developed a simulation model for MAF process to predict the interface temperature and validated this model with experimental results. It was predicted that temperature ranged between 34–51 °C. Mulik et al. [28] measured temperature by using K type thermocouples and obtained the maximum temperature value of 46 °C during experiments for UAMAF process which is taken as the material temperature in this study. Table 4 summarizes various temperatures involved in the same equation for calculating shear stress.

By taking average rake angle as the rake angle due to half depth of cut, shear angle is estimated based on the maximum shear stress and minimum total energy concept of Ernst and Merchant by the following equation [16]:

$$\varnothing = (\pi/4) - [(\beta - \alpha)/2] \tag{40}$$

The coefficient of friction for shearing region is also taken equal to the coefficient of friction for ploughing region. Hence,

$$\tan\beta = \mu_p \tag{41}$$

While estimating the sheared area of work-piece due to a bulge, it is assumed that only frontal surface of the bulge is involved in shearing, back surface is indented in the work-piece due to normal force but not involved in the shearing process. Shearing force on the bulge is calculated as

$$f_{sx} = \tau_s A_s \tag{42}$$

$$\text{Total area under shear and plough for } a \text{ bulge} = A_s + A_p = \pi r_b t \tag{43}$$

Therefore,

$$A_s = \pi r_b t - \pi r_b t_p = \pi r_b (t - t_p) \tag{44}$$

As the number of bulges on a single SiC particle indented in the work-piece is n_b, the shear force on an SiC particle is given as

$$\dot{f}_{sx} = n_b \tau_s A_s \tag{45}$$

Similarly, ploughing force per SiC particle in horizontal direction $\dot{f}_{px}$ can be calculated by multiplying n_b to f_{px}. Therefore, the finishing torque due to a single particle (T_g) which is positioned at a radius of r_n in its circular track can be calculated as

$$\vec{T_g} = \vec{r_n} \times (\vec{\dot{f}_{sx}} + \vec{\dot{f}_{px}}) \tag{46}$$

For calculating the position of SiC particles in bottom layer, it is assumed that there is a uniform distribution of active SiC particles along the length and width of all the electromagnet poles. If n_l and n_w be the number of active SiC particles along the length and width of pole respectively, the ratio of n_l and n_w is equal to the ratio of length and width of poles of electromagnet. As total number of active SiC particles is N_{SiC} under all four poles,

$$n_l \times n_w = N_{SiC}/4 \tag{47}$$

For simplification, it is also assumed that all particles are arranged in circular tracks as shown in Fig. 7(b, c). If the distance between two SiC particles on adjacent tracks is d, the distance between the particles on first track and nth track can be calculated using an arithmetic progression series. This distance between the particles on first track and last track is equal to the length of pole. Hence, the distance between

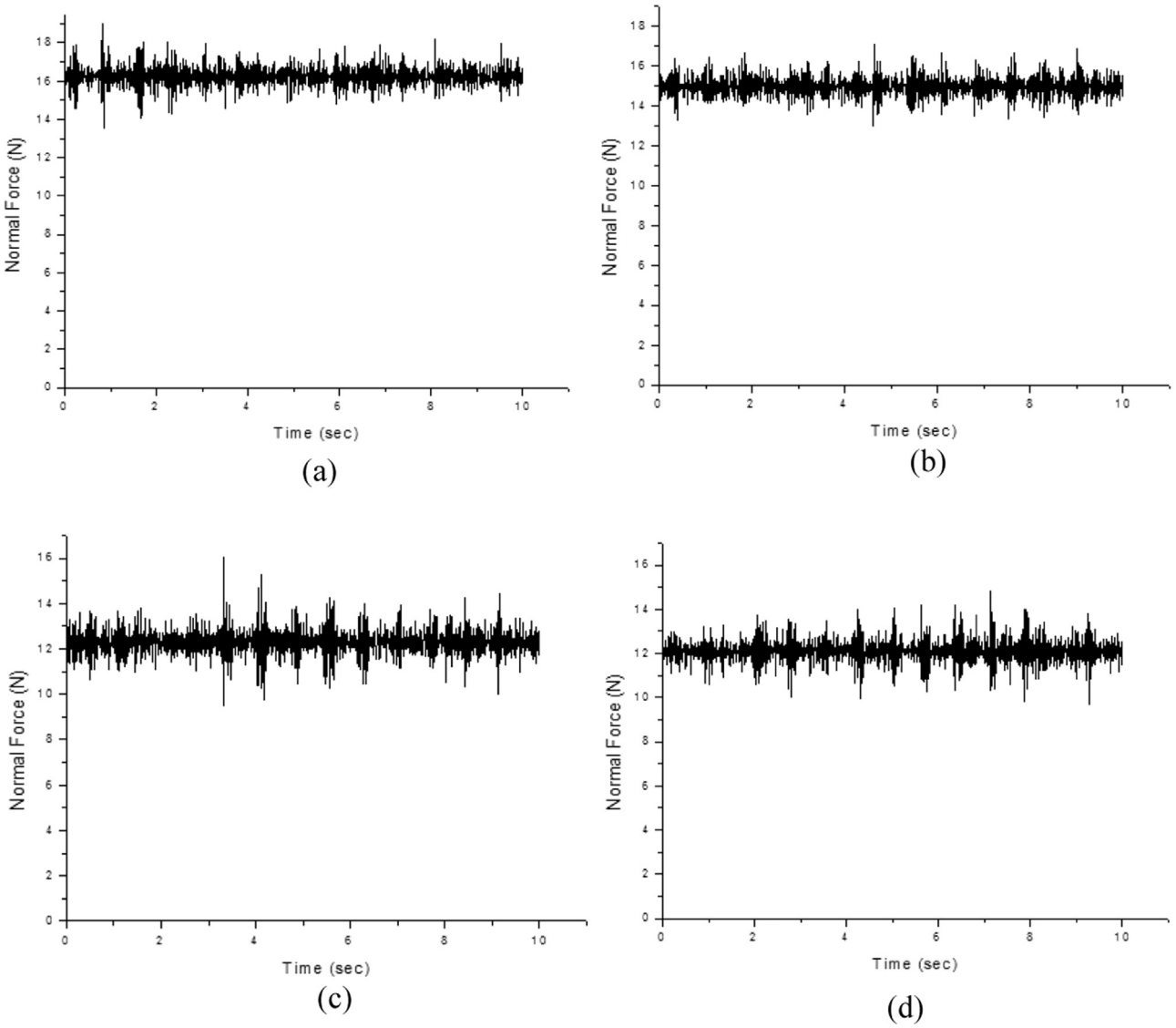

Fig. 10. Experimental values of normal force at different working gaps (in mm): (a) 1.0 (b) 1.5 (c) 2.0 (d) 2.5.

two particles on adjacent tracks d can be determined from

$$n_l(n_l - 1)d/2 = \text{length of pole} \tag{48}$$

Therefore, the total finishing torque (T_f) can be determined by summing up the entire domain in the finishing zone of magnetic poles over the radius of the magnetic brush and is expressed by

$$T_f = \sum_{1}^{N_{SiC}} T_g \tag{49}$$

4. Results and discussions

Finishing experiments were performed on SS304 work material and the material removal and wear pattern during UAMAF process were studied. Comprehensive analysis of surface integrity of the workpiece by the UAMAF process was done with the help of scanned electron microscopy (SEM) and atomic force microscopy (AFM) micrographs. Also, under different process conditions, force and torque were measured to validate the results obtained by the mathematical model with experimental results.

4.1. Surface morphological studies

Experimental investigations were carried to study the surface peaks removal and wear mechanism and also to establish the presence of ploughing phenomenon. For this purpose, the work samples were finished under different process conditions. SEM and AFM images of unfinished and finished workpieces were taken and compared to understand the changes in the surface morphology. Fig. 8 compares the surface profiles of the unfinished and finished surfaces. It can be observed that UAMAF process removed the lays from the surface effectively which were present in the unfinished surface. The images for finished surfaces show the new pattern of lays in Fig. 8(b), (c) and (d). Presence of ploughing effect is established in Fig. 8(c) and (d) whereas ploughing effect does not seem to be predominating in Fig. 8(b). The surface profile achieved in Fig. 8(b) was at $z = 0.8$ mm, $I = 1.1$A which resulted in considerably better surface finish as compared to the work surfaces shown in Fig. 8(c) and (d). This is easy to understand that at lower working gap of 0.8 mm and higher current of 1.1 A, the magnetic field generated was high that enabled the magnetic abrasive powder to form a sufficiently strong FMAB. This condition led the abrasive particles to make deep penetration into the work surface and wear out the peaks easily. Since the chains of FMAB finishing the work surface were firmly attached to the electromagnet due to higher magnetic field, this

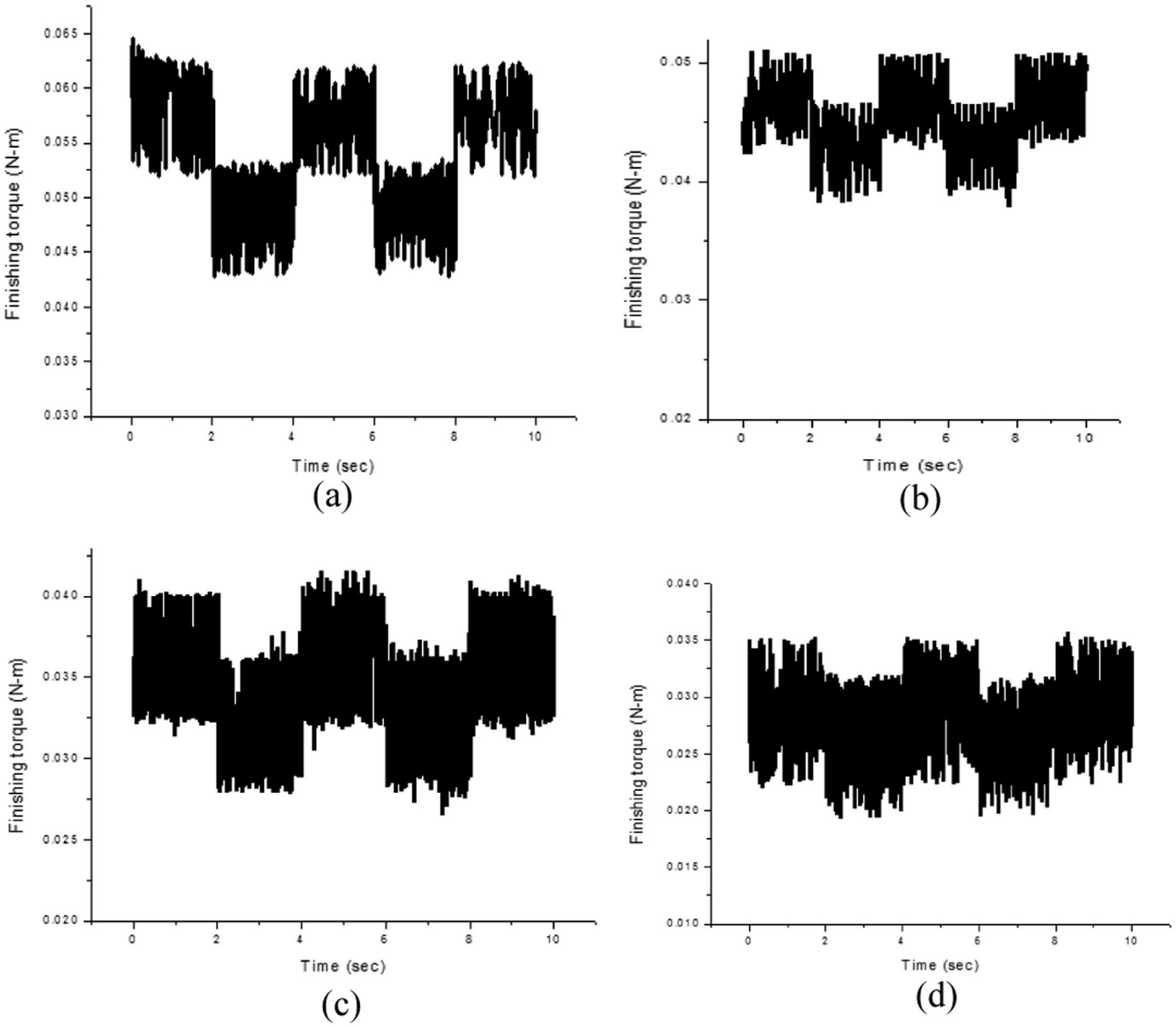

Fig. 11. Experimental values of finishing torque at different working gaps (in mm): (a) 1.0 (b) 1.5 (c) 2.0 (d) 2.5.

Table 5
Validation of normal force and finishing torque.

S.No.	Working gap z (mm)	Predicted Value		Experimental Value		% error in	
		F_y (N)	T_f (Nm)	F_y (N)	T_f (Nm)	F_y	T_f
1.	1.0	18.27	0.0566	16.80	0.0543	8.75	4.24
2.	1.5	16.38	0.0457	14.95	0.0434	9.57	5.30
3.	2.0	14.32	0.0373	12.80	0.0343	11.88	8.75
4.	2.5	13.37	0.0308	12.40	0.0278	7.82	10.79

Table 6
Validation of normal force and finishing torque.

S.No.	Current I (A)	Predicted Value		Experimental Value		% error in	
		F_y (N)	T_f (Nm)	F_y (N)	T_f (Nm)	F_y	T_f
1.	0.9	14.80	0.0375	14.01	0.0358	5.64	4.75
2.	1.0	18.27	0.0566	16.80	0.0543	8.75	4.24
3.	1.1	22.11	0.0823	20.30	0.0760	8.92	9.82
4.	1.2	26.31	0.1160	23.82	0.1060	10.45	9.43

material removal model acted like a two-body wear mechanism. This wear mechanism enabled the abrasive particles to slide on the work surface resulting in more wear rate. Since the strong FMAB rotated for a finishing time of 5 min continuously, the plastically ploughed material was easily abraded due to high wear rate and finished the work surface with presence of less ploughing zone. In case of the images shown in Fig. 8(c) and (d), the working gap was kept more and the current supplied was less in comparison to the previous case. Due to this, the magnetic field generated in these cases were relatively modest, which led to the formation of moderate FMAB. Hence, electromagnet along with FMAB, active abrasive particles and work surface made three different bodies during finishing process. This situation made the abrasive particles free to slide and roll on the work surface like three body wear mechanism which resulted in relatively less surface finish and more chances of occurrence of ploughing effect as compared to the case depicted in Fig. 8(b).

AFM images were also taken for unfinished and finished work surface to observe the ploughing effect. AFM micrograph for unfinished surface in Fig. 9(a) shows a large number of peaks present on the surface. It is seen that the peaks upto 240.8 nm were present in unfinished work surface. Fig. 9(b) and (c) shows micrographs for two finished samples with surface roughness of 44.9 nm and 49.4 nm. The micrographs for finished surface also establish that both sheared and

ploughed surfaces were present after the finishing process.

4.2. Experimental investigations into normal force and finishing torque

To validate the analytical model developed for UAMAF process, a number of experiments were done on SS304 work material. The effect of parameters working gap (z) and current (I) were observed on the force and torque and compared with the predicted values from the model. Experimental values of normal force and torque were measured with the help of dynamometer; different plots of force and torque were drawn with respect to time and shown in Figs. 10 and 11. Force and finishing torque at constant rpm of electromagnet were measured using dynamometer. Table 5 provides comparison between the predicted and experimental values of force and finishing torque by varying working gap at fixed current (I = 1 A, T_{on} = 2 s and T_{off} = 2 s):

Another comparison was made between the predicted and experimental values of force and finishing torque by varying current and keeping fixed working gap (z = 1 mm, T_{on} = 2 s and T_{off} = 2 s) as detailed in Table 6.

The effect of variation in z on F_y and T_f can be noted from Table 5. It is observed as the gap increased, both F_y and T_f decreased. This is clear to understand that more working gap reduces flux density entering the work piece. Reduced flux density produces low magnetic normal force and torque. When the gap was kept constant, increase in F_y and T_f was observed on increasing the current to the electromagnet as summarized in Table 6. This happened because more value of current increased the value of polishing pressure applied on the work piece which in turn increased the force and torque. The effect of ultrasonic vibrations on T_f was also reflected in Fig. 11 where fluctuation in torque after each 2 s time interval is noticed. This observation is justified as the ultrasonic vibrations are applied to the work piece with on and off time of 2 s. It is also seen that theoretical values of normal force and finishing torque are more than experimental values. It may be due to the assumption made in theoretical modeling that there is no flux leakage or copper loss; however, such types of phenomenon occur in actual practice.

5. Conclusions

Mathematical modeling of normal force and finishing torque for UAMAF process using sintered MAP has been developed considering shearing and ploughing effects. The presence of ploughing along with shearing effect is also confirmed by SEM and AFM images of the finished work surfaces. The effect of ultrasonic vibrations is studied. Johnson-cook model is used to estimate the shear strength.

The wear mechanism involved in the removal of surface peaks is explained with the help of SEM and AFM micrographs. It is found that active abrasives were in close contact with FMAB at low working gap and high supply current due to the formation of strong FMAB. This situation finished the surface as per two body wear mechanism. This wear mechanism also enabled the UAMAF process to finish the surface with the presence of small ploughing zone. However, three body wear mechanism was involved during the finishing process with high working gap and low current. This situation also gave a freedom to active abrasives for sliding as well as rolling, which led to predominance of ploughing effect with less wear rate.

Experimental results obtained for the force and torque validate the accuracy level of the results of theoretical model. It is noted that the accuracy ranges from 5.64%–11.88% in case of normal force and 4.24–10.79% in case of finishing torque. These predicted values are good in agreement with experimental values. The main reason for the variations in values is due to flux leakage and copper losses, which are ignored in theoretical models.

Acknowledgements

This work has been carried out under EPSRC (UK)-DST (India) sponsored project 'MAST: Modeling of Advanced Materials for Simulation of Transformative Manufacturing Processes'(Grant identifications: EP/K028316/1 and DST/RC-UK/14-AM/2012). The authors extend sincere thanks to the sponsors for supporting this research.

References

[1] S.C. Jayaswal, V.K. Jain, P.M. Dixit, Modeling and simulation of magnetic abrasive finishing process, Int. J. Adv. Manuf. Technol. 26 (2005) 477–490.
[2] M. Fox, K. Agrawal, T. Shinmura, R. Komanduri, Magnetic abrasive finishing of rollers, Ann. CIRP 43 (1) (1994) 181–184.
[3] V.C. Shukla, P.M. Pandey, Experimental investigations into sintering of magnetic abrasive powder for ultrasonic assisted magnetic abrasive finishing process, Mater. Manuf. Process. 32 (2017) 108–114.
[4] R.S. Mulik, P.M. Pandey, Mechanism of surface finishing in ultrasonic-assisted magnetic abrasive finishing process, Mater. Manuf. Process. 25 (2010) 1418–1427.
[5] A.K. Singh, S. Jha, P.M. Pandey, Mechanism of material removal in ball end magnetorheological finishing process, Wear 302 (2013) 1180–1191.
[6] R.S. Mulik, P.M. Pandey, Experimental investigations and modeling of finishing force and torque in ultrasonic assisted magnetic abrasive finishing, J. Manuf. Sci. Eng. 134 (2012) 1–12.
[7] P. Kala, P.M. Pandey, Experimental study on finishing forces in double disk magnetic abrasive finishing process while finishing paramagnetic workpiece, Procedia Mater. Sci. 5 (2014) 1677–1684.
[8] H.W. Park, S.Y. Liang, R. Chen, Microgrinding force predictive modelling based on microscale single grain interaction analysis, Int. J. Manuf. Technol. Manag. 12 (2007) 25–38.
[9] H.W. Park, S.Y. Liang, Force modeling of micro-grinding incorporating crystallographic effects, Int. J. Mach. Tools Manuf. 48 (2008) 1658–1667.
[10] H. Sin, N. Saka, N.P. Suh, Abrasive wear mechanisms and the grit size effect, Wear 55 (1979) 163–190.
[11] S.M. Son, H.S. Lim, J.H. Ahn, Effects of the friction coefficient on the minimum cutting thickness in micro cutting, Int. J. Mach. Tools Manuf. 45 (2005) 529–535.
[12] P.K. Basuray, B.K. Misra, G.K. Lal, Transition from ploughing to cutting during machining with blunt tools, Wear 43 (1977) 341–349.
[13] A. Popov, A. Dugin, A comparison of experimental estimation methods of the ploughing force in orthogonal cutting, Int. J. Mach. Tools Manuf. 65 (2013) 37–40.
[14] D.J. Waldorf, R.E. DeVor, S.G. Kapoor, An evaluation of ploughing models for orthogonal machining, Trans. ASME 121 (1999) 550–558.
[15] D. Germain, G. Fromentin, G. Poulachon, S. Bissey-Breton, From large-scale to micro machining: a review of force prediction models, J. Manuf. Process. 15 (2013) 389–401.
[16] S. Sikder, H.A. Kishway, Analytical model for force prediction when machining metal matrix composite, Int. J. Mech. Sci. 59 (2012) 95–103.
[17] V. Singh, P.V. Rao, S. Ghosh, Development of specific grinding energy model, Int. J. Mach. Tools Manuf. 60 (2012) 1–13.
[18] A. Ghosh, A.K. Mallik, Manufacturing Science, East-West Press Pvt Ltd, New Delhi, 2003.
[19] V.C. Shukla, P.M. Pandey, Comprehensive study for optimizing sintered density of magnetic abrasive particles of Fe and SiC mix for UAMAF process, IVth International Conference on Production and Industrial Engineering, CPIE-2016, December 19 – 21, NIT Jalandhar, India.
[20] T. Mori, K. Hirota, Y. Kawashima, Clarification of magnetic abrasive finishing mechanism, J. Mater. Process. Technol. 143–144 (2003) 682–686.
[21] R. Transchel, F. Heini, J. Stirnimann, F. Kuster, C. Leinenbach, K. Wegener, Influence of the clearance angle on the cutting efficiency of blunt, octahedral-shaped diamonds in an active filler alloy, Int. J. Mach. Tools Manuf. 75 (2013) 9–15.
[22] N. Ikawa, S. Shimada, H. Tanaka, G. Ohmori, Atomistic analysis of nanometric chip removal as affected by tool-work interaction in diamond turning, Ann. CIRP 40 (1991) 551–554.
[23] G.R. Johnson, W.H. Cook, A constitutive model and data for metals subjected to large strains, high strain rates and high temperatures, in: Proceedings of the 7th International Symposium on Ballistics 541-547, 1983.
[24] C. Nath, M. Rahman, Effect of machining parameters in ultrasonic vibration cutting, Int. J. Mach. Tools Manuf. 48 (2008) 965–974.
[25] C. Zhang, S. Yuan, M. Amin, H. Fan, Q. Liu, Development of a cutting force prediction model based on brittle fracture for C/SiC in rotary ultrasonic facing milling, Int. J. Adv. Manuf. Technol. 85 (2016) 573–583.
[26] A.K. Gupta, H.N. Krishnamurthy, Y. Singh, K.M. Prasad, S.K. Singh, Development of constitutive models for dynamic strain aging regime in Austenitic stainless steel 304, Mater. Des. 45 (2013) 616–627.
[27] V. Mishra, H. Goel, R.S. Mulik, P.M. Pandey, Determining work-brush interface temperature in magnetic abrasive finishing process, J. Manuf. Process. 16 (2) (2014) 248–256.
[28] R.S. Mulik, V. Srivastava, P.M. Pandey, Experimental investigations and modeling of temperature distribution in the work-brush interface during ultrasonic assisted magnetic abrasive finishing process, Mater. Manuf. Process. 27 (2012) 1–9.